Published in final edited form as:
J Micromech Microeng. 2010 ; 20(2): 25008. doi:10.1088/0960-1317/20/2/025008.

Aluminum nitride on titanium for CMOS compatible piezoelectric transducers

Joseph C Doll[1], **Bryan C Petzold**[1], **Biju Ninan**[2], **Ravi Mullapudi**[2], and **Beth L Pruitt**[1]
[1]Department of Mechanical Engineering, Stanford University, Stanford, CA, USA
[2]Tango Systems, San Jose, CA, USA

Abstract

Piezoelectric materials are widely used for microscale sensors and actuators but can pose material compatibility challenges. This paper reports a post-CMOS compatible fabrication process for piezoelectric sensors and actuators on silicon using only standard CMOS metals. The piezoelectric properties of aluminum nitride (AlN) deposited on titanium (Ti) by reactive sputtering are characterized and microcantilever actuators are demonstrated. The film texture of the polycrystalline Ti and AlN films is improved by removing the native oxide from the silicon substrate *in situ* and sequentially depositing the films under vacuum to provide a uniform growth surface. The piezoelectric properties for several AlN film thicknesses are measured using laser doppler vibrometry on unpatterned wafers and released cantilever beams. The film structure and properties are shown to vary with thickness, with values of d_{33f}, d_{31} and d_{33} of up to 2.9, −1.9 and 6.5 pm V^{-1}, respectively. These values are comparable with AlN deposited on a Pt metal electrode, but with the benefit of a fabrication process that uses only standard CMOS metals.

1. Introduction

High-speed, low-power actuators and sensors find numerous applications in microelectromechanical systems (MEMS). Although electrostatic parallel plate and comb drives are widely used for their simplicity, piezoelectric actuators are ideal for applications such as high-speed atomic force microscopy [1], nanoscale electromechanical switches [2], resonators [3] and RF filters [4]. Zinc oxide (ZnO) and lead zirconium titanate (PZT) are commonly used piezoelectric materials, but they pose a contamination risk in tools shared with CMOS fabrication processes and can be difficult to process (e.g. low resistivity, composition control, cracking) [5]. In contrast, aluminum nitride (AlN) is CMOS compatible and can be deposited by several methods, including reactive sputtering. While the d_{33} piezoelectric response of AlN is less than that of ZnO or PZT [5], its other material properties (e.g. high elastic modulus and thermal conductivity, low density) make it ideal for many applications. The deposition of AlN on metal electrodes has been studied extensively for thin film bulk acoustic resonator (FBAR) applications [6]. Although post-CMOS compatible processes have been presented [7–9], they utilize nonstandard metals (e.g. Cr, Mo, Pt) which limits their process compatibility in many common situations. A deposition and fabrication method for AlN using only standard CMOS metals would enable new applications for piezoelectric transducers in nano- and microscale integrated systems.

pruitt@stanford.edu.
Online at stacks.iop.org/JMM/20/025008

The piezoelectric properties of polycrystalline AlN are derived from columnar grains with (0 0 2) crystal orientation. Metals that have been shown to yield reproducibly good AlN texture (e.g. Mo, Pt) are distinguished from other electrode materials (e.g. Ti, Al) partly by their small degree of lattice mismatch with AlN [10]. Metal electrode crystal planes which present hexagonal orientation for the growth of wurtzite AlN include Al (1 1 1), Pt (0 0 2), Ti (0 0 2) and Mo (1 1 0). Although the lattice mismatch of AlN with Ti and Pt is comparable, Pt has yielded better performance to date [11]. Exposure of the bottom electrode to oxygen has been shown to affect AlN grain structure and polarity [12], and an amorphous layer of AlN precedes columnar growth when deposited on TiO_2 [13]. These results suggest that the piezoelectric response of AlN on Ti can be improved by investigating the surface condition of the deposition substrate.

In this paper, we report a deposition and fabrication process for AlN piezoelectric transducers on silicon using only standard CMOS metals. We have previously reported preliminary characterization results [14]. AlN is deposited by pulsed dc reactive sputtering on a silicon substrate using Ti as the electrode metal. We studied the dependence of film properties on processing parameters and found that the AlN film texture is improved by sequentially depositing the films under vacuum and *in situ* cleaning to remove surface oxides to yield a uniform AlN nucleation surface. Using laser doppler vibrometry on unpatterned wafers and microfabricated cantilevers, we measured d_{33f} and d_{31} values of 2.9 and −1.9 pm V^{-1}, respectively. These values correspond to a d_{33} value of up to 6.5 pmV^{-1}, comparable to results obtained for AlN on Pt.

2. Microfabrication

Cantilevers were fabricated from 4 inch (1 0 0) silicon-on-insulator (SOI) wafers (5 μm device layer, 500 nm buried oxide, 500 μm handle). The fabrication process is presented in figure 1. After defining the alignment marks, the piezoelectric film stack is uniformly deposited on the wafer. The stack consists of an AlN interlayer (≈140 nm), Ti bottom electrode (≈85 nm), AlN actuation layer (200–1700 nm) and top Ti electrode (≈275 nm). The top Ti electrode is lithographically patterned and etched (50:1 H_2O:HF), and then used as a hard mask to pattern the AlN actuation layer (25% TMAH, room temperature). The bottom Ti electrode and AlN interlayer are patterned and etched using identical processes. The lithographic mask for the bottom Ti and AlN was designed to encompass and protect the top Ti and AlN layers. The cantilevers are patterned in the (1 0 0) direction in the silicon device layer by deep reactive ion etching (DRIE). After the frontside of the wafer is protected by a thick photoresist layer, the handle of the wafer is patterned and etched with DRIE from the backside and the buried oxide is removed by CHF_3/O_2 RIE to release the cantilevers.

We chose to use Ti rather than Al for the metal electrodes for its greater performance and process compatibility. Ti (0 0 2) has less lattice mismatch (5%) with AlN than Al (1 1 1) (23%), reducing strain near the film interface [10]. Etch selectivity between AlN, the electrode metal and the Si substrate is also required. Room temperature tetramethylammonium hydroxide (TMAH) etches both Al and AlN [8], but neither Ti nor Si. Thus, it is possible to etch the AlN with TMAH and the Ti with hydrofluoric acid (HF) without affecting the underlying Si substrate, whereas Al and AlN can not be selectively etched with respect to each other.

Scanning electron micrographs (SEMs) of finished devices are shown in figures 2(*a*) and (*b*). Minimal undercut of the AlN is observed from the room temperature TMAH etch, as has been reported previously [8].

3. AlN deposition

The AlN and Ti films were deposited in a pulsed dc reactive sputter deposition system (Tango Systems, San Jose, CA). Power, pressure and substrate temperature for AlN deposition were held constant at 5 kW, 5 mTorr and 200 °C, respectively. The temperature and pressure were chosen to minimize N incorporation into the Ti and instrinsic stress in the AlN [11]. Target–substrate distance was fixed at 45 mm. The chamber was evacuated to a base pressure of 10^{-8} Torr before the sputtering. The AlN deposition rate was 21.2 nm min^{-1} with Ar and N_2 flow rates maintained at 10 sccm and 40 sccm, respectively. The AlN deposition parameters are summarized in table 1. All Ti films were sputtered at 3 kW with 40 sccm Ar to yield a deposition rate of 40 nm min^{-1}.

For surface condition studies, the Si substrate was cleaned by either an inductively coupled plasma (ICP) at 800 W bias for 150 s or sputtered at 800 W for 100 s. Both options utilize an Ar flow rate of 40 sccm and remove approximately 50 Å from the surface. The ICP cleaning was performed in a separate chamber from the sputtering chamber. Vacuum was maintained while transferring wafers from the ICP chamber to the PVD chamber. The Ti and AlN depositions were isolated through sputtering shields to control cross-contamination.

We utilized an AlN interlayer below the bottom metal electrode as demonstrated by Kamohara *et al* [15]. This yields large piezoelectric coefficients and isolates the bottom electrode from the substrate to reduce cross-talk with other electronic devices on the same die. A cross-section SEM of the AlN is presented in figure 2(*c*), showing the columnar orientation of the AlN grains.

4. Device and film characterization

The AlN films were characterized using several methods. X-ray diffraction (XRD) θ–2θ and rocking curve scans were used to assess the AlN orientation and film texture (Philips X'Pert Pro, 45 kV, 40 mA). Rocking curves were measured by first performing a θ–2θ scan to find the AlN (0 0 2) reflection peak (2θ = 36.04°) and then with 2θ fixed, varying the wafer holder angle (ω) to measure the degree of grain alignment normal to the wafer. The reflected x-ray intensity was measured with a parallel plate collimator and sealed proportional detector. X-ray photoelectron spectroscopy (XPS) (SSI S-Probe XPS Spectrometer, 10 kV, 150 × 800 μm area) was used to quantify the AlN elemental composition after sputtering a 2 × 2 mm area to remove surface contamination and the top Ti electrode. Scanning electron microscopy (SEM) in combination with focused ion beam milling was used to obtain electron micrographs and measure all film thicknesses (FEI Strata 235 DB). The measured film thicknesses are summarized in table 2 and are used in the d_{31} calculations.

We measured the d_{33f} piezolectric coefficient at the wafer scale and the d_{31} coefficient at the device scale with a laser doppler vibrometer (LDV) (Polytec OFV-2500) as shown in figure 3. Although double-beam interferometry is typically used to measure d_{33f} in piezoelectric thin films, LDV was recently demonstrated [16]. The d_{33f} coefficient at the wafer scalewas measured by biasing the AlN film across its thickness and measuring the induced deflection of the top surface (figure 3(*a*)). In order to avoid exciting the bending modes of the wafer and to improve the LDV displacement resolution, we opted to drive the wafer at significantly higher frequencies (800 kHz–1.2MHz) than have been utilized previously (8 kHz) [17].

For whole wafer laser doppler vibrometry measurements, the wafers were coated with an additional layer of Ti on the backside to improve electrical contact and firmly fixed in place with adhesive. We measured the bias voltage across the AlN film with a separate set of electrodes to account for the output impedance of the amplifier and the low impedance of the AlN at high frequency. The amplitude of the bias voltage and LDV output were recorded with

a spectrum analyzer (HP 3562A), and the change in film thickness was calculated from the measured velocity and driving frequency.

The d_{33f} coefficient is calculated from

$$d_{33f}=\frac{\epsilon_3}{E_3}=\frac{\Delta t}{V_{\text{bias}}} \tag{1}$$

where ϵ_3 and E_3 are the strain and electric field in the piezoelectric film in the out-of-plane direction, Δt and V_{bias} are the change in the thickness of the piezoelectric film and the electric potential applied across it.

The thin film piezoelectric coefficient (d_{33f}) is smaller than the actual piezoelectric coefficient of the material (d_{33}) due to the clamping effect of the thick Si substrate [18]. The d_{33} coefficient is related to d_{33f} and d_{31} by

$$d_{33}=d_{33f}+\frac{2s_{13}^E}{s_{11}^E+s_{12}^E}|d_{31}| \tag{2}$$

where the elastic compliance parameters s_{11}^E, s_{12}^E and s_{13}^E are taken from [19], which correspond to E_{11} = 396 GPa, E_{12} = 137 GPa and E_{13} = 108 GPa.

The d_{31} coefficient was extracted by sinusoidally biasing the unimorph cantilever actuators and measuring the tip deflection for multiple applied voltages in order to calculate the corresponding d_{31} coefficient. The cantilever actuators were also biased with a square wave in order to unambiguously determine the sign of the piezoelectric coefficients from the direction of cantilever tip motion. We tested two cantilever beam designs: a 30 μm wide × 100 μm long × 5 μm thick Si cantilever with a 26 μm × 96 μm AlN stack, and a 50 μm wide × 200 μm long × 5 μm thick Si cantilever with a 30 μm × 196 μm AlN stack. The multilayered cantilever structure was modeled following the methods outlined in [20,21] using the film thicknesses measured by SEM (table 2) and the material properties in table 3. The longitudinal axis of the cantilever beam design is in the (1 0 0) direction and the material properties were chosen for that crystallographic orientation. The cantilevers were actuated at a frequency approximately 100 times below their resonant frequency to avoid dynamic effects. The non-negligible cantilever beam width was accounted for by using the transformations $E \rightarrow E/(1-\nu^2)$ and $d_{31} \rightarrow d_{31}(1+\nu)$ in the calculations as described in [21].

5. Results and discussion

We first investigated the effect of the Si substrate surface condition on the AlN microstructure. Previous work indicated that Ti (1 0 0) rather than (0 0 2) is obtained when an oxidized Si substrate is used [22]. Removing the native SiO_2 by *in situ* inductively coupled plasma (ICP) improved the AlN and Ti orientation in comparison with presputtered or untreated Si substrates (figure 4). The AlN (0 0 2) and Ti (0 0 2) peaks were both substantially increased by the removal of the native SiO_2 from the surface. The AlN exhibited pure (0 0 2) alignment, without any other observable orientations.

Next we investigated the effect of AlN film thickness on the degree of grain alignment. The rocking curve full-width at half-maximum (FWHM) was found to depend inversely upon the film thickness as expected (figure 5). Increasing the RF-induced bias from 45 V to 57 V modestly improved the FWHM for an AlN film thickness of≈400 nm, while reducing the bias

from 45 V to 40 V almost doubled the FWHM from <3° to 5.5° for a film thickness of≈1700 nm. These values are slightly greater than previous reports of 2.6° [23] for AlN on Ti with an AlN interlayer. Although our rocking curve FWHM is larger than reported values for Pt and Mo (<2°), Tonisch *et al* [24] found that a narrow rocking curve is essential for acoustic resonator performance but much less so for general transducers.

Film texture is an indirect measurement of the AlN piezoelectric response because the formation of both parallel and anti-parallel grains can lead to a negligible piezoelectric response despite good apparent film alignment [25]. Ruffner *et al* [12] found that allowing the bottom metal electrode to oxidize before depositing the AlN film led to a change in the polarity and a reduction in the magnitude of the piezoelectric response. Akiyama *et al* [26] observed a similar trend by controlling the concentration of oxygen. However, they attributed the change in polarity to Al–O binding in the plasma rather than at the surface.

In light of the potential importance of oxygen concentration, we characterized the composition of the AlN films with XPS. We removed the top Ti electrode by Ar sputtering and found the composition of the AlN to be O = 6.4% ± 1.6%, N = 37.8% ± 1.8%, Al = 54.0% ± 2.2% (n = 6, $\mu \pm \sigma$) (figure 6). The measured oxygen concentration agrees well with earlier measurements of peak piezoelectric response by Akiyama *et al* [26]. However, we measured a high concentration of both aluminum and oxygen in the AlN film, in contrast with the hypothesis in [26] that a high oxygen concentration necessarily corresponds to a depletion of aluminum in the film.

One interpretation of these results is that oxygen affects the AlN piezoelectric response by two mechanisms: substrate oxidation and bulk oxidation. At low concentration when the substrate is not uniformly oxidized, the piezoelectric response decreases and can vanish due to the mixture of + and − grain polarities. At high concentration, the piezoelectric response is reduced by oxygen-induced grain defects. XRD rocking curve measurements will be affected by the second effect but not the first. In general, grain polarity is a complex function of many parameters including surface condition and a polarity change can be induced by varying the deposition pressure [27] or power [28]. Accordingly, it is necessary to directly measure both the sign and magnitude of the piezoelectric response rather than try to infer them from the film structure. The film morphology of AlN on Ti has been reported [22,29], but the piezoelectric response has been less frequently measured [11,23]. We measured the piezoelectric properties of the films we deposited by two separate methods: d_{33f} at the wafer scale and d_{31} using microfabricated cantilevers.

We determined the sign of the piezoelectric coefficients by biasing the AlN on the cantilever beams with a square wave. By observing the direction of cantilever tip deflection we could determine whether d_{33} is positive or negative. The cantilever tip initially deflects upward in response to a positive bias on the top electrode, indicating $d_{33} > 0$ and $d_{31} < 0$ (figure 7(*a*)). This is in contrast with Ruffner *et al* and is in agreement with Dubois and Muralt [11], although different deposition conditions were used in each study. By exciting the piezoelectric film with white noise we measured resonant frequencies within 10% of the expected value and quality factors between 300 and 600. When sinusoidally biasing the cantilever actuators the tip deflection amplitude varied linearly with bias voltage as expected (figure 7(*b*)). For a fixed voltage amplitude, a thinner piezoelectric film leads to greater tip deflection due to the increased magnitude of the electric field.

The d_{33f} and d_{31} coefficients were measured for each film thickness at multiple bias voltage amplitudes and frequencies. The measured piezoelectric coefficients are inversely proportional to the rocking curve FWHM (figure 8). For film thicknesses of 200 nm, 400 nm and 1700 nm we measured d_{33f} of 2.37 ± 0.44, 2.47 ± 0.37 and 2.91 ± 0.31 pm V^{-1} (n = 21, 3 wafers) and

d_{31} of −1.08 ± 0.06, −0.96 ± 0.21 and −1.91 ± 0.55 (n = 264, 8 cantilevers). The d_{33} coefficient for the 1700 nm thick film is approximately 6.50 pm V^{-1}, using equation (2). Overall, the piezoelectric coefficients we measured are greater than previously reported data for AlN on Ti [11] (d_{33f} = 2.3 pm V^{-1}), and compare well with those for epitaxial AlN on sapphire (d_{31} = −2.6 pm V^{-1}) [30] and AlN on Pt (d_{33} = 6.8 pm V^{-1}) [18].

These material properties are sufficient for many high speed microactuator applications such as high-speed AFM or nanomechanical switches. The tip deflection and resonant frequency for a 250 μm long cantilever beam operating at a bias voltage of 10 V is plotted against cantilever beam thickness for the fabricated and characterized AlN actuator thicknesses (figures 9(*a*) and (*b*)). As the cantilever beam becomes thinner or longer, the resonant frequency decreases while the tip deflection increases. Performance can be approximated as independent of beam width assuming that the piezoelectric covers the entire beam. Deflections up to several microns are possible while maintaining a resonant frequency >20 kHz. It is also possible to increase the resonant frequency to several MHz for tip deflections of ≈50 nm.

A possible figure of merit for high-speed MEMS cantilever actuator applications is the product of resonant frequency and tip deflection, which is independent of cantilever length in our model, and is plotted in figure 9(*c*). The frequency-deflection product can be increased in several possible ways. The piezoelectric film quality can be improved to increase the d_{31} coefficient, leading to increased tip deflection for the same resonant frequency. Alternatively, the electric field can be increased by reducing the thickness of the piezoelectric film or increasing the bias voltage. However, care must be taken in reducing the film thickness because both the resonant frequency and d_{31} coefficient will decrease slightly. Finally, the thickness of non-piezoelectric layers such as the silicon substrate can be reduced until the neutral axis intersects the piezoelectric layer and the tip deflection begins to decrease. In certain applications, it possible to use a bimorph rather than unimorph actuation configuration to nearly eliminate non-piezoelectric layers and further increase the frequency-deflection product [31].

6. Conclusion

AlN thin films have been fabricated on Ti electrodes with excellent piezoelectric properties for CMOS compatible MEMS applications. Our results suggest that *in situ* substrate pre-cleaning and sequential deposition of films under vacuum limits surface oxide formation, improving the uniformity of the AlN grain polarity and maximizing the piezoelectric response. We characterized the piezoelectric properties of the films with LDV using both whole wafers and released cantilevers, achieving d_{33f} (2.9 pm V^{-1}) and d_{31} (−1.9 pm V^{-1}) coefficients comparable to AlN on Pt, but with a fabrication process that utilizes only standard CMOS metals and is compatible with surface and bulk Si micromachining.

Acknowledgments

Fabrication work was performed in part at the Stanford Nanofabrication Facility (a member of the National Nanotechnology Infrastructure Network) supported by the NSF under grant ECS-9731293, its lab members and the industrial members of the Stanford Center for Integrated Systems. This work was supported by the National Institutes of Health under grant EB006745, and the National Science Foundation (NSF) under CAREER Award ECS-0449400 and COINS NSF-NSEC ECS-0425914.

References

1. Sulchek T, Hsieh R, Adams JD, Minne SC, Quate CF, Adderton DM. High-speed atomic force microscopy in liquid. Rev. Sci. Instrum 2000;71:2097–2099.

2. Mahameed R, Sinha N, Pisani MB, Piazza G. Dual-beam actuation of piezoelectric ALN RF MEMS switches monolithically integrated with ALN contour-mode resonators. J. Micromech. Microeng 2008;18:105011.
3. Cleland AN, Pophristic M, Ferguson I. Single-crystal aluminum nitride nanomechanical resonators. Appl. Phys. Lett 2001;79:2070–2072.
4. Piazza G, Stephanou PJ, Pisano AP. Piezoelectric aluminum nitride vibrating contour-mode MEMS resonators. J. Microelectromech. Syst 2006;15:1406–1418.
5. Trolier-McKinstry S, Muralt P. Thin film piezoelectrics for MEMS. J. Electroceramics 2004;12:7–17.
6. Ruby RC, Bradley P, Oshmyansky Y, Chien A, Larson JD III. Thin Film Bulk Wave Acoustic Resonators (FBAR) for Wireless Applications 2001;vol 1:813–821.
7. Kim HH, Ju BK, Lee YH, Lee SH, Lee JK, Kim SW. A noble suspended type thin film resonator (STFR) using the SOI technology. Sensors Actuators A 2001;89:255–258.
8. Saravanan S, Berenschot E, Krijnen G, Elwenspoek M. A novel surface micromachining process to fabricate AlN unimorph suspensions and its application for RF resonators. Sensors Actuators A 2006;130–131:340–345.
9. Andrei A, Krupa K, Jozwik M, Delobelle P, Hirsinger L, Gorecki C, Nieradko L, Meunier C. AlN as an actuation material for MEMS applications: the case of AlN driven multilayered cantilevers. Sensors Actuators A 2008;141:565–576.
10. Lee J-B, Jung J-P, Lee M-H, Park J-S. Effects of bottom electrodes on the orientation of AlN films and the frequency responses of resonators in AlN-based FBARs. Thin Solid Films 2004;447–448:610–614.
11. Dubois M-A, Muralt P. Stress and piezoelectric properties of aluminum nitride thin films deposited onto metal electrodes by pulsed direct current reactive sputtering. J. Appl. Phys 2001;89:6389–6395.
12. Ruffner JA, Clem PG, Tuttle BA, Dimos D, Gonzales DM. Effect of substrate composition on the piezoelectric response of reactively sputtered AlN thin films. Thin Solid Films 1999;354:256–261.
13. Liu W-J, Wu S-J, Chen C-M, Lai Y-C, Chuang C-H. Microstructural evolution and formation of highly c-axis-oriented aluminum nitride films by reactively magnetron sputtering deposition. J. Cryst. Growth 2005;276:525–533.
14. Doll JC, Petzold BC, Ninan B, Mullapudi R, Pruitt BL. A high d33 CMOS compatible process for aluminum nitride on titanium. 2009 IEEE Transducers. 2009
15. Kamohara T, Akiyama M, Ueno N, Nonaka K, Tateyama H. Growth of highly c-axis-oriented aluminum nitride thin films on molybdenum electrodes using aluminum nitride interlayers. J. Cryst. Growth 2005;275:383–388.
16. Herdier R, Jenkins D, Dogheche E, Remiens D, Sulc M. Laser doppler vibrometry for evaluating the piezoelectric coefficient d_{33} on thin film. Rev. Sci. Instrum 2006;77:093905–093915.
17. Wang Z, Miao J. Critical electrode size in measurement of d_{33} coefficient of films via spatial distribution of piezoelectric displacement. J. Phys. D: Appl. Phys 2008;41:035306.
18. Martin F, Muralt P, Dubois M-A, Pezous A. Thickness dependence of the properties of highly c-axis textured AlN thin films. J. Vac. Sci. Technol. A 2004;22:361–365.
19. Wright AF. Elastic properties of zinc-blende and wurtzite AlN, GaN, and InN. J. Appl. Phys 1997;82:2833–2839.
20. DeVoe DL, Pisano AP. Modeling and optimal design of piezoelectric cantilever microactuators. J. Microelectromech. Syst 1997;6:266–270.
21. Weinberg MS. Working equations for piezoelectric actuators and sensors. J. Microelectromech. Syst 1999;8:529–533.
22. Sanz-Hervas A, Vergara L, Olivares J, Iborra E, Morilla Y, García-López J, Clement M, Sangrador J, Respaldiza MA. Comparative study of c-axis AlN films sputtered on metallic surfaces. Diam. Relat. Mater 2005;14:1198–1202.
23. Kamohara T, Akiyama M, Ueno N, Nonaka K, Kuwano N. Influence of aluminum nitride interlayers on crystal orientation and piezoelectric property of aluminum nitride thin films prepared on titanium electrodes. Thin Solid Films 2007;515:4565–4569.
24. Tonisch K, Cimalla V, Foerster Ch, Romanus H, Ambacher O, Dontsov D. Piezoelectric properties of polycrystalline AlN thin films for MEMS application. Sensors Actuators A 2006;132:658–663.

25. Clement, M.; Vergara, L.; Olivares, J.; Iborra, E.; Sangrador, J.; Sanz-Hervas, A.; Zinck, C. SAW and BAW response of c-axis AlN thin films sputtered on platinum. Ultrasonics Symposium IEEE; 2004. p. 1367-1370.

26. Akiyama M, Kamohara T, Kano K, Teshigahara A, Kawahara N. Influence of oxygen concentration in sputtering gas on piezoelectric response of aluminum nitride thin films. Appl. Phys. Lett 2008;93:021903–021913.

27. Kamohara T, Akiyama M, Ueno N, Sakamoto M, Kano K, Teshigahara A, Kawahara N, Kuwano N. Influence of sputtering pressure on polarity distribution of aluminum nitride thin films. Appl. Phys. Lett 2006;89:243507.

28. Kamohara T, Akiyama M, Kuwano N. Influence of polar distribution on piezoelectric response of aluminum nitride thin films. Appl. Phys. Lett 2008;92:093506.

29. Iriarte GF, Bjurstrom J, Westlinder J, Engelmark F, Katardjiev IV. Synthesis of c-axis-oriented AlN thin films on high-conducting layers: Al, mo, ti, TiN, and ni. IEEE Trans. Ultrason. Ferroelectr. Freq. Control 2005;52:1170–1174. [PubMed: 16212256]

30. Tsubouchi K, Mikoshiba N. Zero-temperature-coefficient SAW devices on AlN epitaxial films. IEEE Trans. Sonics Ultrason 1985;32:634–644.

31. Sinha N, Wabiszewski GE, Mahameed R, Felmetsger VV, Tanner SM, Carpick RW, Piazza G. Piezoelectric aluminum nitride nanoelectromechanical actuators. Appl. Phys. Lett 2009;95:053106.

32. Wortman JJ, Evans RA. Young's modulus, shear modulus, and poisson's ratio in silicon and germanium. J. Appl. Phys 1965;36:153–156.

33. Tsuchiya T, Hirata M, Chiba N. Young's modulus, fracture strain, and tensile strength of sputtered titanium thin films. Thin Solid Films 2005;484:245–250.

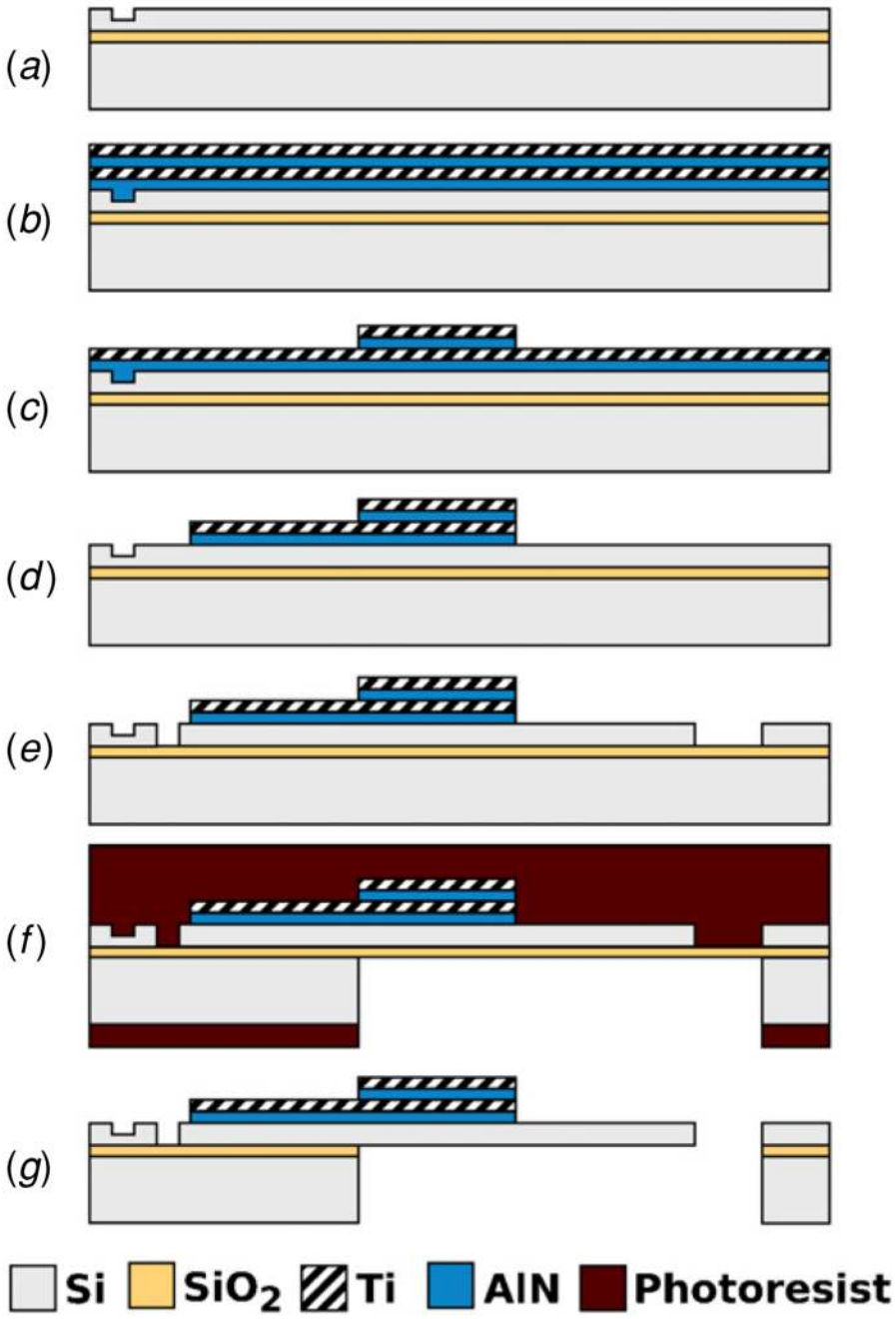

Figure 1.
The fabrication process. (*a*) First the alignment marks are defined and (*b*) the piezoelectric stack is deposited. (*c*) Next, the top Ti electrode is lithographically patterned and wet etched in hydrofluoric (HF) acid. The patterned Ti then acts as a hard mask to etch the AlN actuation layer (200–1700 nm thick) at room temperature TMAH, which dissolves photoresist. (*d*) The same process is repeated for the bottom Ti electrode and AlN interlayer (140 nm thick). (*e*) The cantilever is defined from the frontside of the wafer by deep reactive ion etching (DRIE). (*f*) The wafer is then lithographically patterned on the backside and etched by DRIE, stopping on the buried oxide. (*g*) Finally, the buried oxide is etched by RIE to release the cantilever.

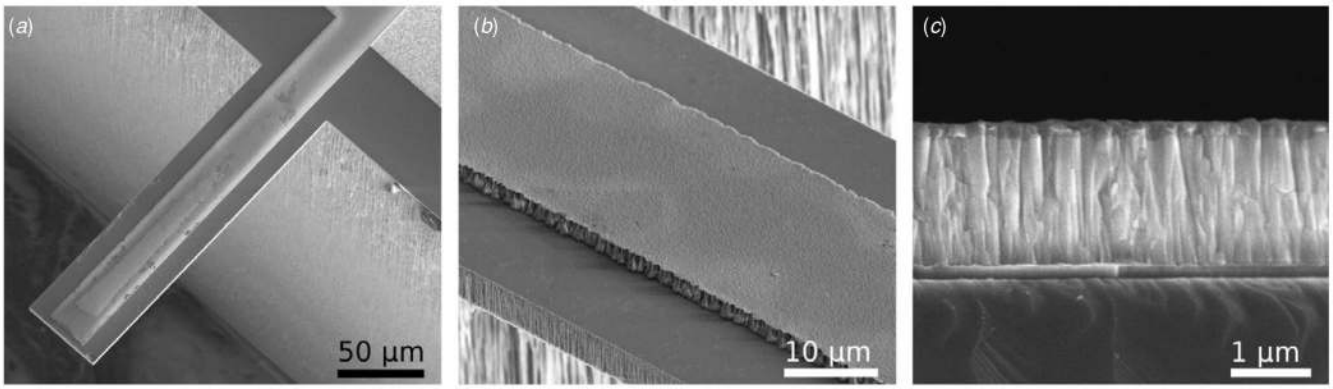

Figure 2.
Scanning electron micrographs of (*a*) a released 5 μm thick × 50 μm wide × 200 μm long cantilever with a 30 μm wide × 196 μm long actuator, (*b*) closeup of the piezoelectric stack showing minimal undercut of the AlN, and (*c*) cross-sectional view of a piezoelectric stack with 1700 nm thick AlN showing the columnar orientation of the AlN grains.

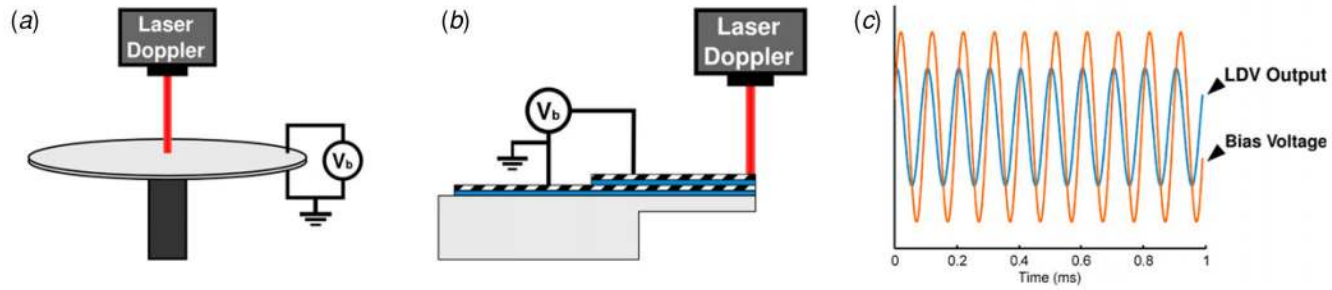

Figure 3.

Experimental setup for measuring d_{33f} and d_{31}. An ac bias voltage is applied across the (*a*) wafer or (*b*) microfabricated cantilever, and the resulting deflection is measured using laser doppler vibrometry. (*c*) The deflection is calculated from the measured velocity and the ratio of bias voltage to displacement is used to calculate the piezoelectric properties of the film.

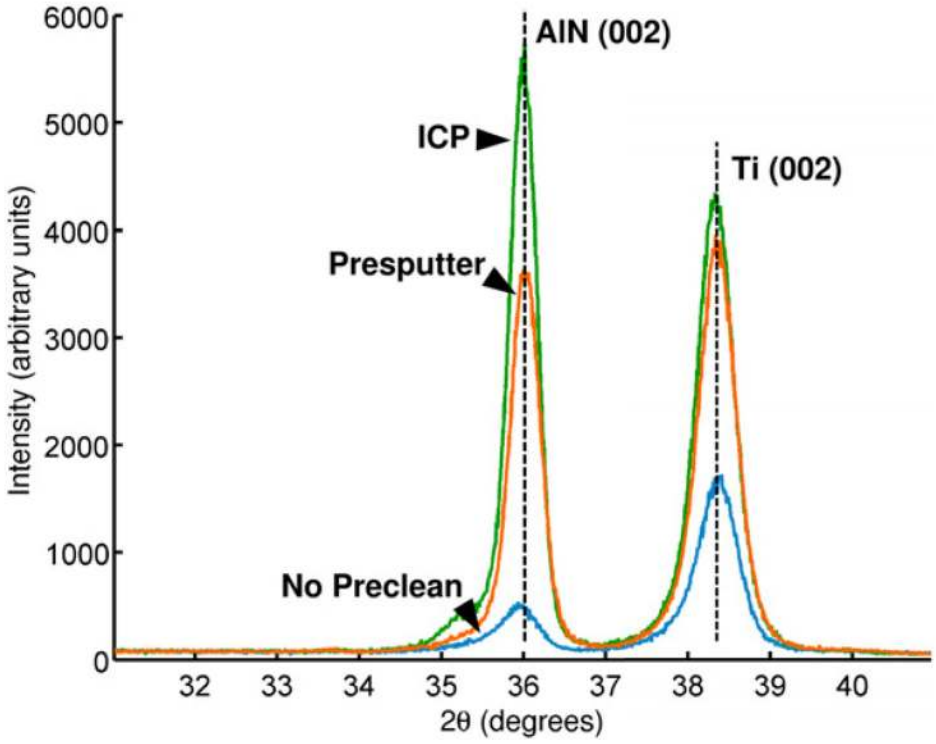

Figure 4.

AlN film texture characterization. (*a*) 100 nm of Ti and 500 nm of AlN were deposited on a Si (1 0 0) substrate in order to investigate the effect of removing the native SiO_2 by presputtering or inductively coupled plasma (ICP). Precleaning the Si substrate *in situ* was found to increase the XRD intensity of the AlN and Ti (0 0 2) peaks. All cleans and depositions were performed in a single vacuum run to prevent the formation of SiO_2 or TiO_2.

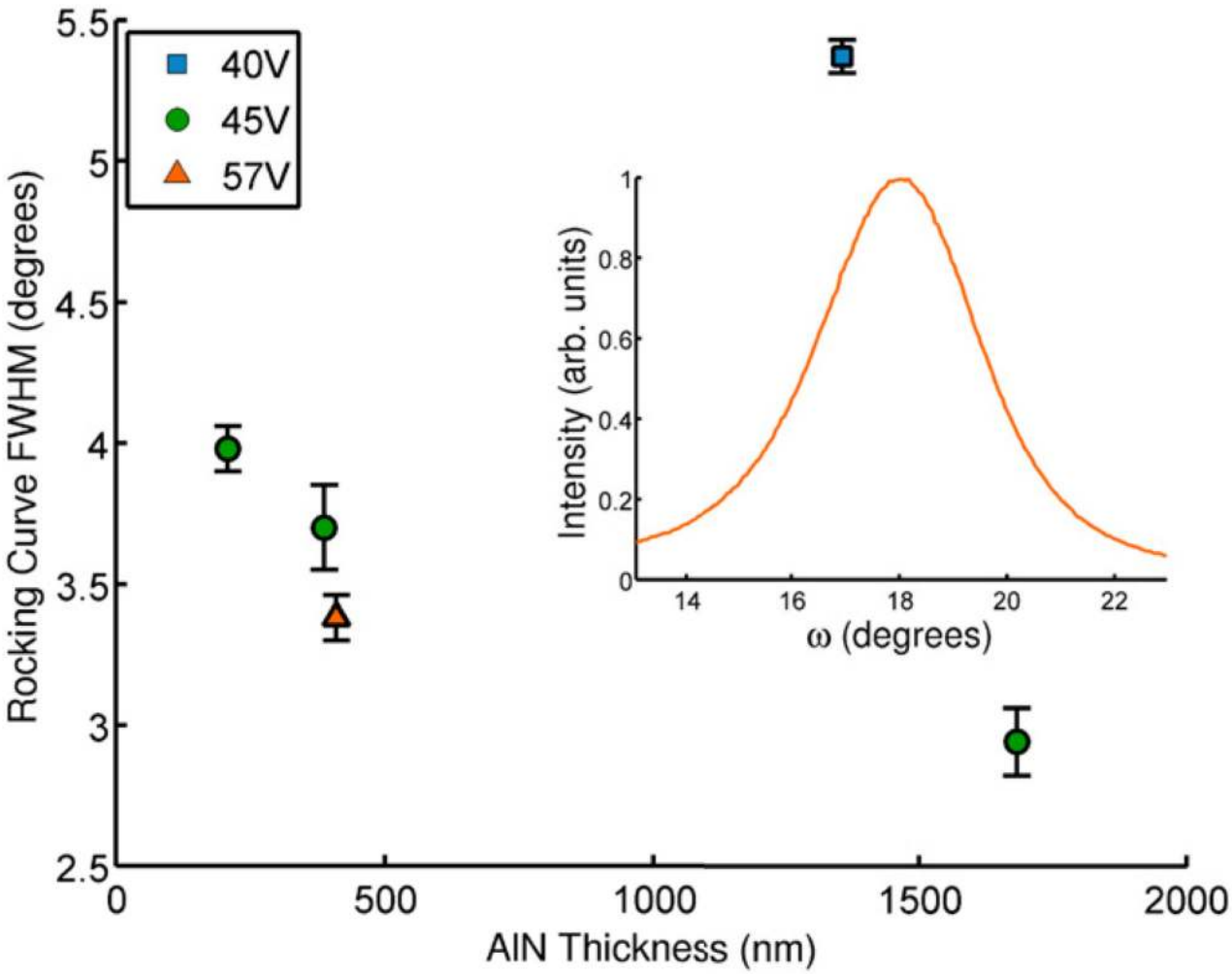

Figure 5.
The XRD rocking curve FWHM of the AlN was found to vary with film thickness. All samples were cleaned by ICP before depositing the AlN/Ti/AlN/Ti film stack ($n = 5$ for each thickness). The orientation uniformity of the AlN (0 0 2) grains was improved by increasing both the film thickness. We investigated the effect of RF-induced bias for several thicknesses and found that increased bias may lead to improved grain alignment. A sample rocking curve is inset (57 V bias).

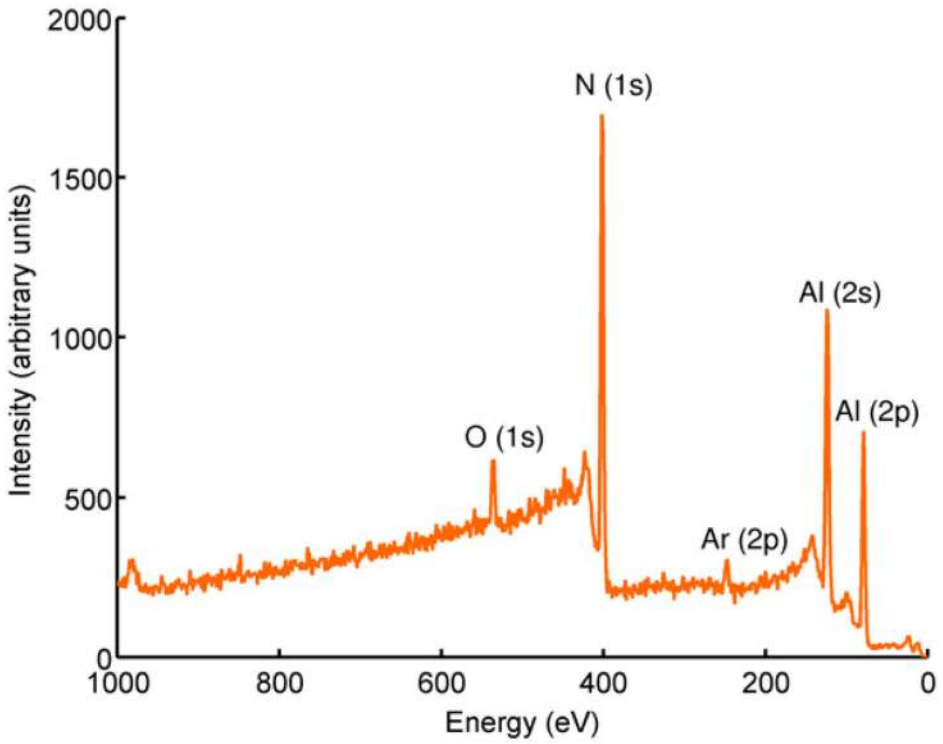

Figure 6.
X-ray photoelectron spectroscopy (XPS) survey scan recorded after removing the top Ti electrode by sputtering. Atomic composition was calculated to be O = 6.4% ± 1.6%, N = 37.8% ± 1.8%, Al = 54.0% ± 2.2% (μ ± σ, n = 6).

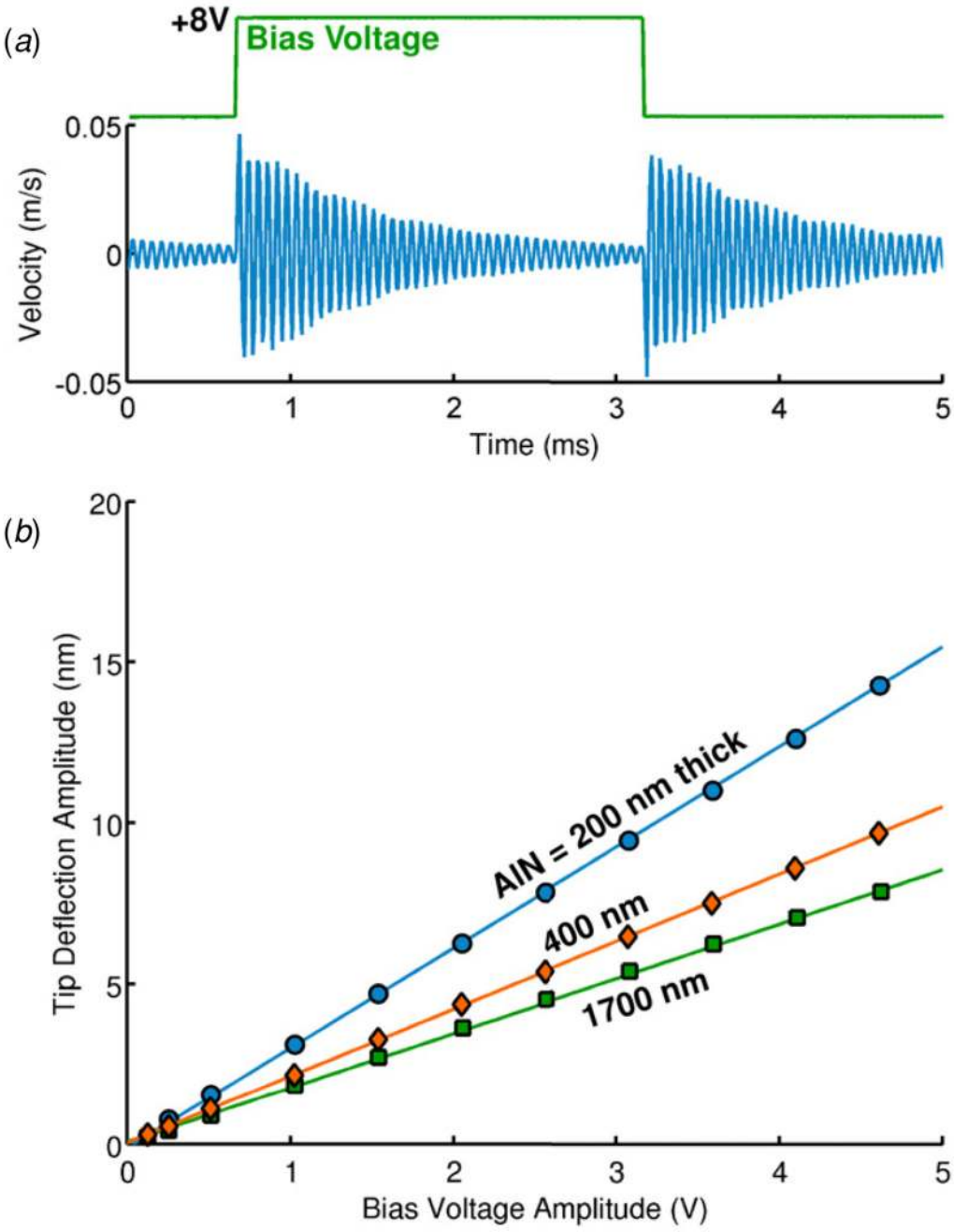

Figure 7.

Cantilever characterization measurements. (a) To determine the sign of the piezoelectric coefficients, the AlN actuator is biased with a square wave and the cantilever tip velocity is measured with LDV. The tip of the cantilevers moves in the +z direction in response to positively biasing the top Ti electrode with respect to the bottom electrode, so $d_{33} > 0$ and $d_{31} < 0$. (b) The magnitude of the piezoelectric response is determined by applying an ac bias to the AlN actuator and measuring the tip deflection amplitude. Example data for 100 μm long cantilevers with several AlN thicknesses is shown. The bias frequency (10 kHz) is much less than the cantilever resonant frequency (550 kHz). For a fixed bias voltage, tip deflection increases as the AlN thickness is reduced due to the larger electric field.

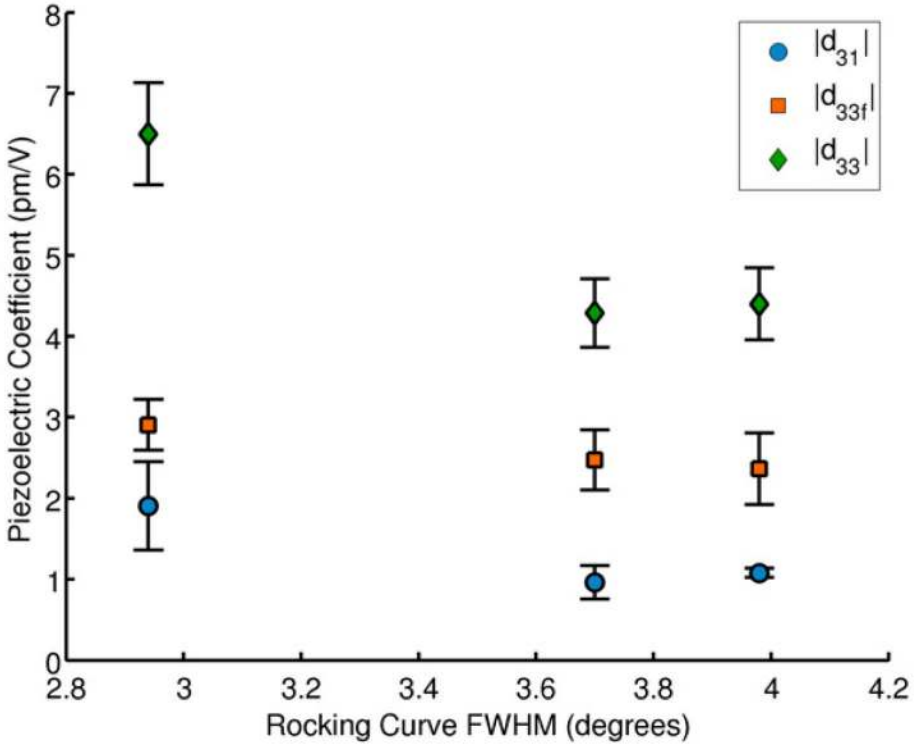

Figure 8.
Dependence of d_{33f} (n = 21, 3 wafers) and d_{31} (n = 264, 8 cantilevers) on the rocking curve FWHM for AlN deposited with an RF-induced bias of 45 V. The d_{33} coefficient is calculated from d_{33f}, d_{31} and the AlN material properties. Both d_{33f} and d_{33} are positive while d_{31} is negative.

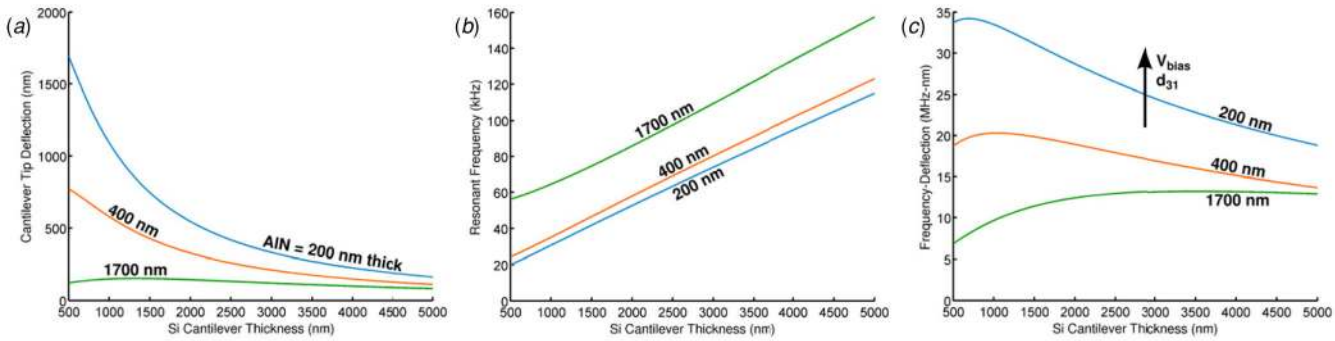

Figure 9.

Analytical (*a*) tip deflection, (*b*) resonant frequency and (*c*) their product as a function of silicon thickness for AlN actuator thicknesses of 200, 400 and 1700 nm. Cantilever length and bias voltage are fixed at 250 μm and 10 V, respectively. The thicknesses of the AlN interlayer and Ti electrodes as well as the d_{31} coefficients for each AlN thickness are equal to those experimentally measured. Tip deflection is maximized by reducing the thickness of the Si and the active AlN actuator layer for a fixed bias voltage. However, this leads to a reduction in resonant frequency. The frequency-deflection product is independent of cantilever length and can be maximized by reducing all film thicknesses, improving film quality or increasing the bias voltage.

Table 1

AlN deposition parameters.

Parameters	Values
Base pressure (Torr)	10^{-8}
Deposition pressure (Torr)	5×10^{-3}
Target power (W)	5000
Substrate bias power (W)	200–400
Substrate bias voltage (V)	40–57
Ar:N_2 flow rate (sccm)	10:40
Substrate temperature (°C)	200
Target-substrate distance (mm)	45
Deposition rate (nm min^{-1})	21.2

Table 2

Measured thicknesses of deposited films ($\mu \pm \sigma$).

Layer	Thickness (nm)	Measurements (N)
Top Ti electrode	166 ± 30	29
AlN actuato	208 ± 11, 388 ± 37, 1683 ± 54	6, 5, 10
Bottom Ti electrode	88 ± 19	26
AlN interlayer	136 ± 23	22

Table 3

Material properties used for calculating d_{31} from experimental data.

Material	E_{100} (GPa)	ν	ρ(kg m^{-3})
AlN	396 [19]	0.33	3200
Si	130 [32]	0.27 [32]	2330
Ti	90 [33]	0.33	4500